Original Article

High cycle fatigue behavior of the IN718/M247 hybrid element fabricated by friction welding at elevated temperatures

CrossMark

Tran Hung Tra [a, *], Motoki Sakaguchi [b]

[a] Nha Trang University, 02 Nguyen Dinh Chieu, Nha Trang, Viet Nam
[b] Tokyo Institue of Technology, 2-12-1, I1-41, Ookayama, Meguro-ku, Tokyo, Japan

ABSTRACT

A hybrid element has been fabricated by friction welding, joining two superalloys Inconel 718 and Mar-M247. The high cycle fatigue behavior of this welded element was investigated at 500 °C and 700 °C. The fabrication could obtain excellent fatigue strength in which the fracture is located in the base metal Mar-M247 side and takes place outside the welded zone. The behavior of the joint under loadings is discussed through a simulation by the numerical finite element method.

© 2016 The Authors. Publishing services by Elsevier B.V. on behalf of Vietnam National University, Hanoi. This is an open access article under the CC BY license (http://creativecommons.org/licenses/by/4.0/).

1. Introduction

In order to take full advantage of the properties of different metals, several hybrid and composite components are fabricated. Only in the way of hybrid fabrications, the designer can use most suitable materials for each part of a given structure. In high temperature applications, if the hybrid superalloy components are successfully developed, they are expected to make a significant contribution to improve the economic efficiency in which they can be taken full advantage of materials with different upper temperature limits. Friction welding is emerging as an attractive method for the fabrication of hybrid superalloy components. It is suitable for joining dissimilar metals with high gamma prime volume fractions like Nickel-based superalloys, which are effectively used in gas turbines, but are considered as being unavoidable by other welding methods [1—3].

The main driving force for the use of welding in aeronautical components is weight savings, relating directly to better economics. The faster a vehicle moves, the bigger the potential savings by reducing weight. Especially, weight saving is much more significant when it is located in the hot section of the turbine engines [4]. There is often a multiplier effect of rapidly moving parts within the overall structure. This is the driving force behind the manufacture of blade-disk or "*blisk*" components. Inconel 718 and Mar-M247 are two suitable superalloys used in disks and blades of gas turbines, respectively [5]. In a conventional turbine stage the blades are mechanically attached to a hub in the disk. This attachment involves interlocking parts that add significantly to the total weight of the rotating parts. Friction welding is expected to join these two superalloys in a single piece named "*blisk*". By this way the hub interlocking mechanism is eliminated and a significant weight saving is regarded in gas turbines [6]. However, it is naturally well known that joining dissimilar metals is generally more challenging than that of similar metals because of differences in the physical, mechanical and metallurgical properties of the base metals to be joined [1,7].

In this work, a bond between forged superalloy Inconel 718 and cast superalloy Mar-M247 was fabricated by friction welding processing. The strength of the welded elements was tested under high cyclic loadings at working temperatures in the range of 500 °C and 700 °C. Due to the mismatch of the properties of the two base alloys, the stress and strain concentration in the welded zone are unavoidable. The stress and strain in the welded zones under the loadings were further studied by simulation using a finite element analysis tool.

---

* Corresponding author.
   E-mail address: tra@ntu.edu.vn (T. Hung Tra).
   Peer review under responsibility of Vietnam National University, Hanoi.

Table 1
Chemical composition of IN718 and MAR-M247 (wt., %).

Composition	Ni	Cr	Co	Mo	W	Ta	Nb	Al	Ti	Fe	Mn	Si	C	B	Zr	Hf
IN 718	52.5	19	–	3	–	–	5.1	0.5	0.9	18.5	0.2	0.2	0.04	–	–	–
Mar-M247	60	8.3	10	0.7	10	3	–	5.5	1	–	–	–	0.14	0.015	0.05	1.5

2. Experimental procedures

The hybrid superalloy element was fabricated by friction welding the cast polycrystalline Mar-M247 superalloy (denoted as M247) and the forged Inconel 718 superalloy (denoted as IN718) in a continuous drive friction welding machine (Hereafter this fabricated hybrid superalloy element is denoted as IMHS). In order to obtain an optimal joint, several primary friction welding processes were carried out where the fabrication parameters, such as the rotation speed, preheating time, compressive normal stress, duration time, upset pressure and upset holding time were varied.

The chemical compositions of the two superalloys are shown in Table 1. The initial average grain sizes of the virgin IN718 and virgin M247 are about 10 μm and 1.0 mm, respectively.

The microstructure was investigated by Scanning Electron Microscopy (SEM). For experimental testing, i.e. for both tensile and fatigue tests, solid cylindrical specimens were machined and extracted from the welded solid cylinder with the welded interface located at the specimen center, as illustrated in Fig. 1(a). The isothermal high cycle fatigue (HCF) tests were conducted at 500 °C and at 700 °C, where the stress range was varied. Micro-Vickers hardness measurements were performed across the interface of the welded specimens by a diamond indentator using a 200 g and 5 s of the indentation loading cycle. All the tests were performed by a servo-electro hydraulic test system under the uniaxial stress-controlled loading conditions in the air. The tensile tests were followed ASTM E8 with the strain rate in the loading of 10^{-3}/s. The fatigue tests were conducted with a symmetric stress range ($R_{\varepsilon} = -1$) and at the frequency of 8.0 Hz (see Fig. 1(b)).

In the IMHS specimens, the welded interface is positioned at the center of the extensometer. The specimens were heated by a high frequency induction heating system. The test temperatures were recorded and controlled through R type thermocouples welded near the specimen shoulder parts (see Fig. 2).

3. Results and discussion

Fig. 3 presents the microstructure of the IMHS in the representative locations. On microscopic scale, there are no visible defects in the welded zone to be recognized. The microstructure in the welded zone indicates significant recrystallization on the IN718 side. The thermo-mechanically affected zone (hereafter called TMAZ) taken on the IN718 side can be clearly seen in this figure

with a significantly coarsened microstructure and the width of about 200 μm. The welded zone on the M247 side shows only unremarkable recrystallization. We note that the base materials M247 and IN718, both show the conventional microstructure. The M247 possesses dendritic structure which consists of considerably large grains in the order of millimeters in diameter. The distribution of the hardness across the weld is shown in Fig. 4. Here a softened zone is formed in an area with approximately a few hundred microns from the welding interface on the IN718 side. In the tensile tests, the specimen was fractured on the M247 side but outside the welded zone. Fig. 5 presents the yield and the tensile strength, respectively, of the specimens tested at room temperature (RT) and at 650 °C. Here the tensile strength of the IMHS tested at room temperature and at 650 °C are comparable to those of the M247. It should be noted that the tensile strength of M247 is lower than that of IN718.

The HCF strength of the IMHS was examined under the HCF loading at 500 °C and at 700 °C. For the results of the HCF tests, all specimens were fractured on the M247 side and the fractured zones were all located outside the welded zone. It is obvious that the strength of the IMHS is higher than that of, at least, the base alloy M247. This result means that the bonding strength between IN718 and M247 in the IMHS is considerably significant under HCF loadings at elevated temperatures. The experimental results of the fatigue tests are displayed in Fig. 6. The fatigue life of the base alloy M247 and that of IN718 are also plotted in this figure for comparison purpose. It can be seen, the life of the IMHS is comparable to that of the base alloy M247. The fatigue strength of the base alloy IN718 is remarkably higher than that of the base alloy M247 and that of the IMHS as well. The coarsened microstructure in the welded zone as seen in Fig. 3(b) is suspected to reduce the fatigue strength of the IN718 in this zone. However, this reduction does not seem considerable in this case.

Under the HCF loadings, the IMHS specimens were fractured in the virgin area of the base alloy M247 side with a traditional fracture mode and thus this work does not focus on the fracture characteristics. The discussion is addressed to the explanation of the fractured locations. Due to the dissimilar properties between the two base metal alloys, namely IN718 and M247, the stress and elastic strain concentration in the welded zone is inevitable. In order to clarify the role of these mismatch properties in the damage of the IMHS under the HCF loadings, the behavior of the IMHS was simulated by a finite element method tool. The total length of the
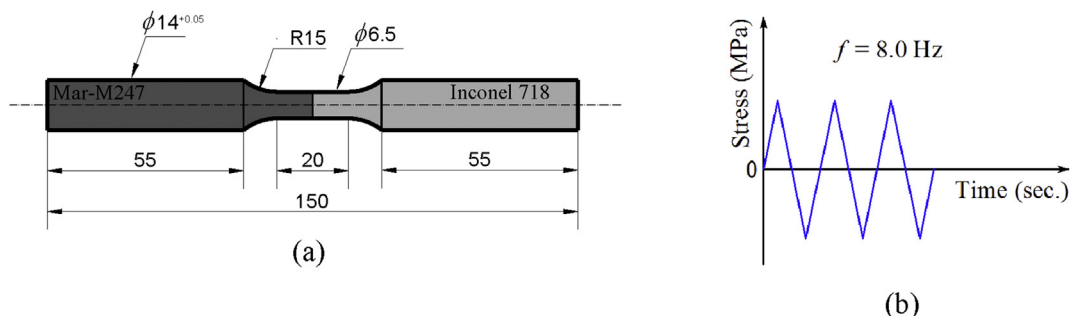

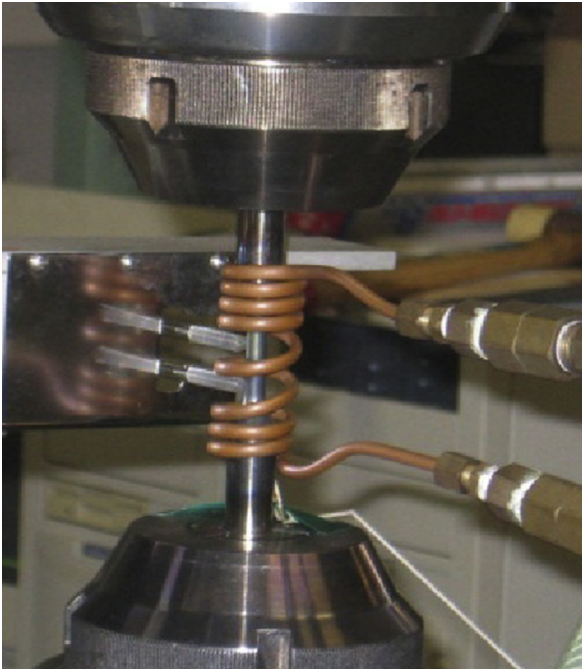**Fig. 1.** (a) The tested specimen geometry and (b) the tested waveform with frequency of 8.0 Hz.

Fig. 2. The fatigue loading tests at high temperature.

model is 12 mm (equal to the length at that the strain gauge was attached to the specimen) whereas the welding interface was located at the center. Based on the microstructure characteristics shown in Fig. 3 and the hardness distribution presented in Fig. 4, it is reasonable to use a model with three layers corresponding to three respective materials, including the virgin IN718 with 5.8 mm

length, the TMAZ of the IN718 with 0.2 mm length, and the virgin M247 with 6.0 mm length as shown in Fig. 7. The analysis model shown in Fig. 7 is just a quarter of an axial cylinder of the IMHS specimen. In this model, two flat surfaces parallel to the axial axis (z axis in Fig. 7) were constrained in displacement symmetry. In the two surfaces perpendicular to the axial axis (z axis in Fig. 7), one was constrained in zero axial displacement (zero displacement in the axial direction) and the other was exposed to the axial load. The constant high temperature was applied to the overall model. The cyclic stress applied in this model was a triangle waveform with a frequency of 8.0 Hz as it was shown in Fig. 1(b) above.

In the meshing, the attention was paid on the refinement at the interface area.

The dash lines named Path No.1, Path No.2, and Path No.3, respectively, in Fig. 7 are the locations used for presenting the analysis results and will be mentioned later. Here, the Path No.1 line is located at the axial centerline of the specimen model, the Path No.2 line is located at a distance of 1.5 mm to the centerline, and the Path No.3 line is located on the model surface.

All materials were assumed to be isotropic and homogeneous. Based on the applied fatigue loadings shown in Fig. 6, the maximum stress in all specimens was found remarkably lower than that of the yield stress of the base alloys and thus it is reasonable to assume the behavior of the materials to be in the range of elasticity. Here, the elastic behavior of the materials was assumed to obey the Hooke's law.

In this work, the Young modulus, tensile properties, and the thermal expansion coefficient of the IN718 and of the M247 were determined from the experiments. For the alloys IN718 and M247 working in the temperature range below 700 °C, a linear dependence of the yield strength on the temperature was assumed and given as: $\sigma_{y(IN718)} = 1105.2 - 0.208 \times T$ and $\sigma_{y(M247)} = 739.6 + 0.016 \times T$, respectively, where the stress is in MPa, and temperature T is in
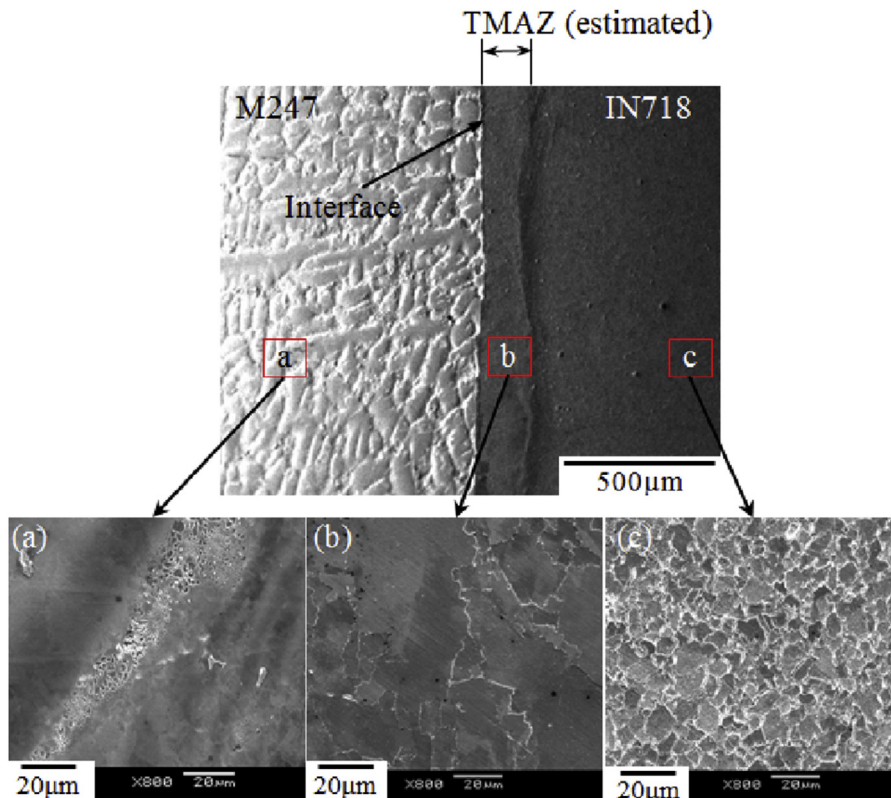

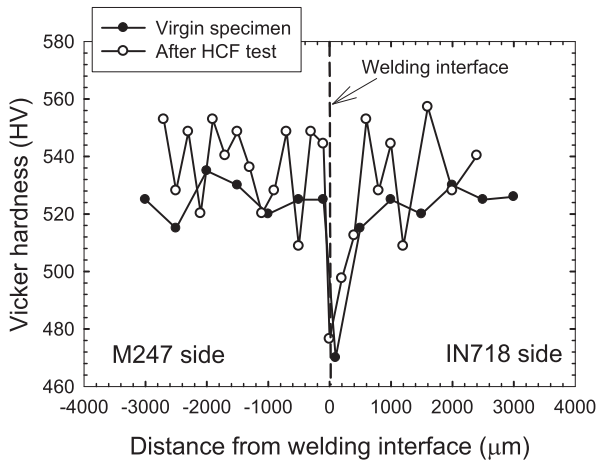Fig. 3. Microstructure in the representative areas in the IMHS.

Fig. 4. Hardness distribution across the element.

degree Celsius. The TMAZ is the thermo-mechanically affected zone on the IN718 side; the material properties such as Poison's ratio (ν), Young modulus (E) and the thermal expansion coefficient (α) of the TMAZ zone are quite acceptable to be similar to those of IN718 [11]. The mechanical properties of the TMAZ must be different from its base alloy IN718. The tensile strength of the TMAZ was assumed to be proportional to the hardness of its base material IN718 [11] for which the measured hardness is shown in Fig. 4. From this view the tensile strength of the TMAZ was estimated to be of about 89% that of IN718. All mechanical properties of IN718, TMAZ, and M247 are summarized in Table 2.

The finite element analysis (FEA) model was examined on convergence and the result was compared with the experimental result. In the Fig. 8, the stress during the cyclic loading from FEA calculation and that measured in the experiment at 700 °C with the cyclic stress amplitude of 220 MPa are presented. The FEA result presented in this figure is the axial stress component (σ_z) of an element located at point *A* in the model (see Fig. 7) which is far from the welding interface. At this location it is expected that the effect of the tri-axiallity stress state in the interface zone induced by the dissimilar properties of the two base metals could be suppressed.

Due to the mismatch of the properties between the two base materials, the stress and strain in and around the welded zone become those of multi-axial states even though the specimen was conducted under the uniaxial loading. The effects of multi-axial stress state on the fatigue damage were investigated in several works and several damage parameters were proposed [14–16]. In this work, a popular fatigue damage parameter proposed by Ali Fatami and Darell F.Socie [14] was introduced in the analysis. This damage parameter is briefly outlined as follows.
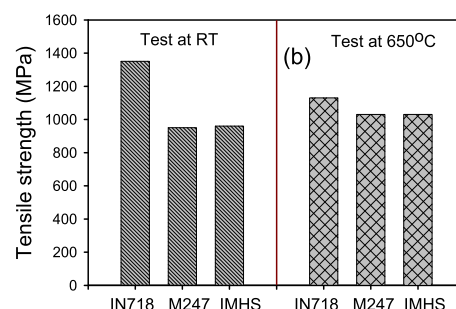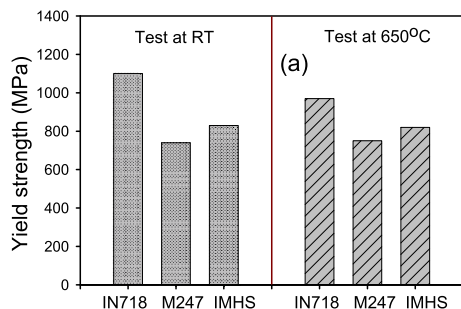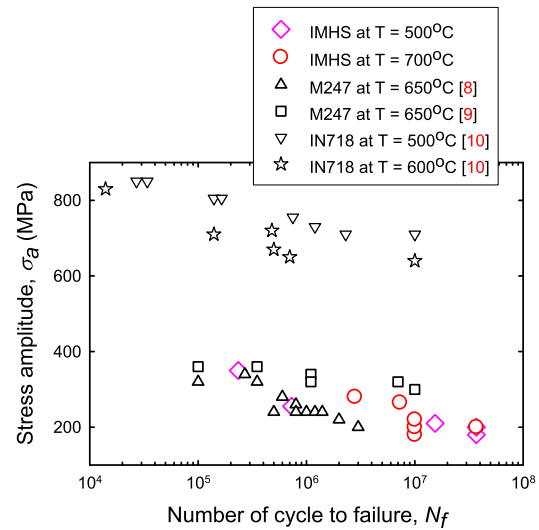

Fig. 6. Fatigue lives of the IMHS and of the two base metals at elevated temperatures [8–10].

Ali Fatami and Darell F.Socie [14] proposed a multi-axial fatigue damage parameter (denoted *FSDP*) defined as

$$FSDP = \gamma_{\max}\left(1 + n\frac{\sigma_n^{\max}}{\sigma_y}\right) = (1 + \nu_e)\frac{\sigma_f'}{E}\left(2N_f\right)^b$$
$$+ \frac{n}{2}(1 + \nu_e)\frac{\left(\sigma_f'\right)^2}{E\sigma_y}\left(2N_f\right)^{2b} + (1 + \nu_p)\varepsilon_f'\left(2N_f\right)^c \quad (1)$$
$$+ \frac{n}{2}(1 + \nu_p)\frac{\varepsilon_f'\sigma_f'}{\sigma_y}\left(2N_f\right)^{b+c}$$

where γ_{max} and $\sigma_n^{\max}$ are maximum shear strain and maximum normal stress on γ_{max} plane; *n* is a constant and $n = 0.6$ [14]; ν_e, ν_p, σ_y, *E* are the elastic Poison's ratio, the plastic Poison's ratio, the yield stress, and the Young modulus, respectively; σ_f', ε_f', *b, c* are respectively the fatigue strength coefficient, the fatigue ductility coefficient, the fatigue strength exponent, and the fatigue ductility exponent, and all these were derived from the uniaxial specimen tests.

The *FSDP* was calculated through γ_{max}, $\sigma_n^{\max}$, *n* and σ_y as mentioned in (Eq. (1)), in which $\gamma_{max} = (\varepsilon_1 - \varepsilon_3)$ and $\sigma_n^{\max} = (\sigma_1 + \sigma_3)/2$. The distribution of the *FSDP* across the model at the end of the tensile loading in a cycle fatigue is displayed in Figs 9 and 10. Fig. 9 shows the distribution of the *FSDP* in Path No.1, Path No.2, and Path No.3 in the fatigue specimen under stress application at an
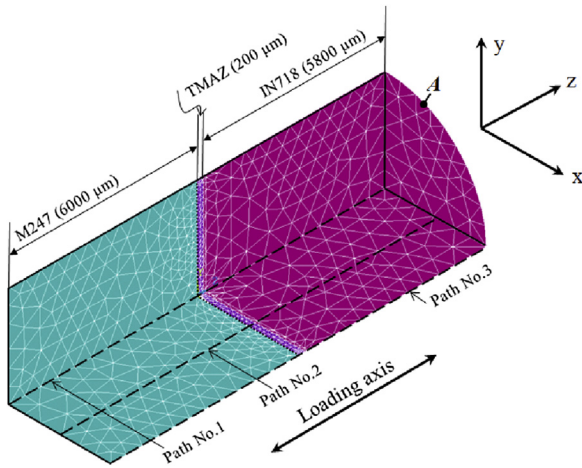

Fig. 5. (a) Yield strength and (b) Tensile strength of the specimens tested at room temperature and at 650 °C.

Fig. 7. The finite element model used for analysis of the IMHS. (The interface is located at the dotted lines).

Table 2
Summary the properties of IN718, TMAZ, and M247.

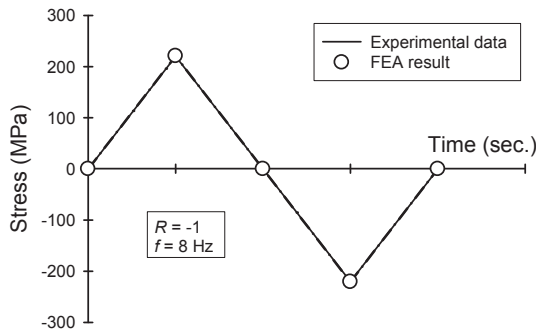|	Young's modulus, E (MPa)	Poisson's ratio, ν	Thermal expansion coef., α (1/°C)
IN718	159,409	0.283 [12]	1.42×10^{-5}
TMAZ	159,409	0.283	1.42×10^{-5}
M247	188,962	0.300 [13]	1.28×10^{-5}

Fig. 8. Comparison between the experimental data and FEA result in a cyclic loading at stress amplitude of 220 MPa tested at 700 °C.
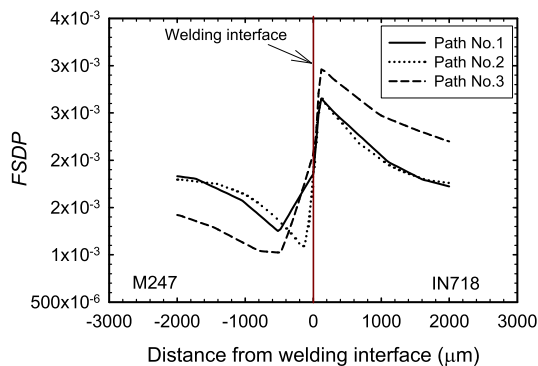

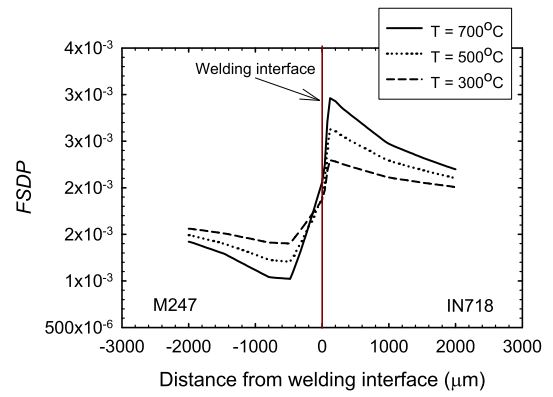Fig. 9. Distribution of the FSDP aross the element on the Path No.1, Path No.2, Path No.3.

Fig. 10. Distribution of the FSDP across the IMHS on the Path No3 at different test temperatures.

amplitude of 220 MPa at 700 °C. The distribution of the FSDP across the model in Path No.3 under the applied stress amplitude of 220 MPa at different testing temperatures is presented in Fig. 10. Generally, the FSDP damage parameter concentrates at the welded zone, near the interface. The FSDP is decreased on the M247 side and increased on the IN718 side. This result means that the fatigue damage in the welded zone on the M247 side is reduced, whilst the fatigue damage in the welded zone on the IN718 side is enhanced. The effect of the mismatch properties between the two base alloys on the fatigue damage on the M247 side seems to be positive. From this view, it might be understood why the fatigue fracture occurred on the M247 side and took place outside the welded zone. The concentration of the FSDP on IN718 side and the coarsened microstructure in the TMAZ (see Fig. 3(b)) on the IN718 side reveal that both the microstructure and the mechanical factor have detrimental effects in the damage of the IMHS on the IN718 side. However, the fatigue strength of the base alloy IN718 is significantly higher than that of the base alloy M247 (see Fig. 6), and the detrimental effects are not high enough to promote the IMHS to be fractured in the welded zone on the IN718 side; and thus, as a result, the fatigue specimens were fractured on the M247 side as it was seen from the experimental tests. It should be noted in Fig. 10 that the higher test temperature, the higher FSDP concentration in the welded zone. In Fig. 11 we present the calculated HCF loading of the elements in the representative areas in the IMHS loaded with a uniaxial stress amplitude of 220 MPa at 700 °C. Here, the vertical axis is presented by the damage parameter FSDP. It can be seen that the cyclic FSDP amplitude at the welded zone on the M247 side is lower than that at the other zones, and that at the welded zone on the IN718 side is higher than that of the other zones. This observation could be considered as a reason for the HCF fractures to
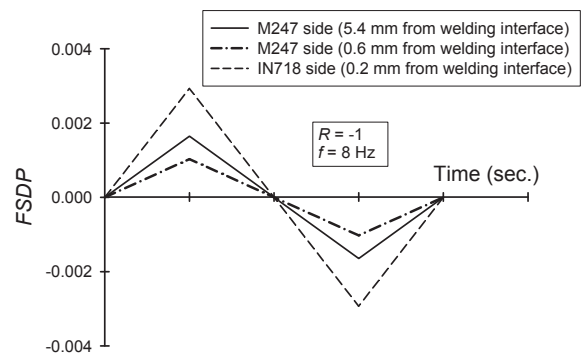

Fig. 11. The cyclic loading result of the elements in the representative zones plotted in term of the multi-axial damage parameter, FSDP.

occur on the M247 side and to take place outside the welded zone of the M247 side.

4. Conclusions

An IMHS element has been fabricated by the friction welding technique. The element displays an excellent strength under HCF loadings at 500 °C and at 700 °C. The IMHS is fractured on the M247 side outside the welded zone. From the numerical simulation results, the multi-axial stress and strain states are presented in and around the welded zone due to the dissimilar properties between the two base alloys. Based on the multi-axial fatigue damage proposed by Fatimi et al., it is found that the fatigue damage in the welded zone on the M247 side is reduced and this damage in the welded zone on the IN718 side is enhanced. The FEA result is satisfactory agrrement with the findings in experimental tests that the specimens were fractured on the M247 side and outside the welded zone.

Acknowledgments

References

[1] John N. DuPont, John C. Lippold, Samuel D. Kiser, Welding Metallurgy and Weldability of Nickel-base Alloys, John Wiley & Sons, Inc, 2009.

[2] Homam Naffakh Moosavy, Mohammad-Reza Aboutalebi, Seyed Hossein Seyedein, Carlo Mapelli, Microstructural, mechanical and weldability assessments of the dissimilar welds between γ′- and γ″-strengthened nickel-base superalloys, Mater. Charact. 82 (2013) 41–49.

[3] F. Daus, H.Y. Li, G. Baxter, S. Bray, P. Bowen, Mechanical and microstructural assessments of RR1000 to IN718 inertia welds - effects of welding parameters, Mater Sci. Tech. 23 (12) (2007) 1424–1432.

[4] Mendez PF, Eagar TW. New trends in welding in the aeronautic industry: http://eagar.mit.edu/EagarPapers/Eagar192.pdf.

[5] Roger C. Reed, The Superalloys Fundamentals and Applications, Cambridge University Press, 2006.

[6] http://www.materials.manchester.ac.uk/our-research/research-impact/friction-welding.

[7] H.Y. Huang, M. Li, M. Preuss, P. Karadge, S. Bowen, G. Bray, Baxter, Inertia friction welding dissimilar Nickel-based superalloys alloy 720Li to IN718, Metall. Mater Trans. A 38 (2007) 1608–1619.

[8] Miroslav Šmíd, Ludvík Kunz, Pavel HutaĜ, Karel Hrbáþek, High cycle fatigue of nickel-based superalloy MAR-M 247 at high temperatures, Procedia Eng. 74 (2014) 329–332.

[9] Domnin Gelmedin, Karl-Heinz Lang, Failure behaviour of the superalloy MAR-M247 LC under LCF, HCF and combined LCF/HCF loading, Int. J. Mater. Res. 103 (No. 1) (2012) 97–105.

[10] N. Kawagoishi, Q. Chen, H. Nisitani, Fatigue strength of Inconel 718 at elevated temperatures, Fatigue Fract. Engng Mater Struct. 23 (2000) 209–216.

[11] Michael F. Ashby, Hugh Shercliff, David Cebon, Materials: Engineering, Science, Processing and Design, Elsevier Ltd, 2007.

[12] Inconel alloy 718, http://www.specialmetals.com/documents/Inconel%20alloy%20718.pdf.

[13] J. Gayda, T. Gabb, Two Dimensional Is Coelastic Stress Analysis of a Prototypical JIMO Turbine Wheel, NASA/TM-2005–213650, 2005.

[14] Fatemi Ali, F. Socie Darrell, A critical plane approaches to multiaxial fatigue damage including out-of-phase loading, Fatigue Fract. Eng. Mater. Struct. 11 (No. 3) (1988) 149–165.

[15] M. Freitas, L. Reis, B. Li, Comparative study on biaxial low-cycle fatigue behavior of three structural steels, Fat. Fract. Eng. Mat. Struct. 29 (2006) 992–999.

[16] Luis Reis, Bin Li, Manuel De, Freitas Multiaxial loadings with different frequencies between axial and torsional components in 42CrMo4 steel, Int. J. Struct. Integr. 1 (No. 4) (2010) 303–313.